Article ID:#54914166. Received: July 28, 2021. Revised: August 25, 202. Accepted: December 21, 2021

Journal of Information and Communication Engineering (JICE), 7 (2): 448-454, December 31, 2021
e-ISSN: 2432-5465, p-ISSN: 2186-9162
Applied Science and Computer Science Publications

Magneto-optical images for nondestructive inspection of plant steel structures using deep generative models

Ryosuke Hashimoto[1], Toshiya Itaya[2], Hiroki Kato[3] Junya Ito[3], Kyoma Nakagawa[3], Hitoshi Nishimura[1] and Syunsuke Fukuchi[1]

National Institute of Technology (Kosen)
Suzuka College, Dept. of Electronic
and Information Engineering, Japan[1]
Email[1]: hashimoto@elec.suzuka-ct.ac.jp

National Institute of Technology(Kosen)
Suzuka College, Dept. of Electronic
and Information Engineering, Japan[2]
Email: itaya@info.suzuka-ct.ac.jp

National Institute of Technology (kosen)
Suzuka College, Advanced Engineering Course
of Science and Technology for Innovation, Japan[3]
and Information Engineering, Japan[3]
Email:hashimoto@elec.suzuka-ct.ac.jp

Abstract: Measures against deterioration of infrastructures that were built during the high economic growth period are facing significant challenges with regard to the maintenance of infrastructures in Japan. The development of optimal nondestructive sensing and imaging technology according to the material and structure of buildings is underway to contribute to efficient and reliable maintenance of infrastructures. However, owing to the large number of materials and structures used for buildings, as well as the types of defects to be targeted, many basic studies are yet to reach the stage of practical use. In this study, we developed a magneto-optical (MO) sensor in order to visualize a "crack" in the plant steel structure and automatically detected the defects in the plant steel structure by performing deep learning on the MO image obtained. As a pretreatment for detecting anomalies in defects using the AI, we focused on the nondestructive inspection using MO imaging and performed an unprecedented image filter processing. As a result, automatically evaluation the several types of MO images using AI, the accuracy of defection identification was improved.

Keywords: artificial intelligence; variational autoencoder, nondestructive inspection; magneto-optical imaging

I. INTRODUCTION

Measures against deterioration of infrastructures that were built during the high economic growth period are facing significant challenges with regard to the maintenance of infrastructures in Japan. Particularly, in response to the ongoing reconstruction and renovation of infrastructure buildings, introducing the latest technology to quantitatively evaluate the life expectancy of the structures is strongly required. The situation allows no time to spare. Given this background, the development of optimal nondestructive sensing and imaging technology according to the material and structure of buildings is underway to contribute to efficient and reliable maintenance of infrastructures. However, owing to the large number of materials and structures used for buildings, as well as the types of defects to be targeted, many basic studies are yet to reach the stage of practical use. In nondestructive inspection of plant steel structures, skilled and experienced engineers judge defects based on images and electrical signals obtained. The authors are conducting a research on innovative nondestructive inspection and have confirmed visualization of defects by a magneto-optical

Corresponding Author: Ryosuke Hashimoto. National Institute of Technology (KOSEN), Suzuka College, Department of Electrical and Electronic Engineering, Shiroko-cho, Suzuka sity, Mie, Japan, Tel: +81-593-68-1800, Fax: +81-593-68-1806, E-mail: hashimoto@elec.suzuka-ct.ac.jp

(MO) imaging [1]-[12], which is based on the MO effect [13]. Deep learning is highly useful method in image processing. By performing deep learning on images obtained from nondestructive inspection using MO imaging, defects of steel can be automatically evaluated, which was earlier done by experienced engineers. In this study, we developed a technology that used an MO element as a sensor to visualize a "crack" in the plant steel structure and automatically detected the defects in the plant steel structure by performing deep learning on the MO image obtained. By defects evaluation in the plant steel structures with artificial intelligence (AI), the work is automated, which contributes to extending the life expectancy of social capital structures in terms of reliability, or whether they need repair. RGB images obtained using a camera have a lot of noise, and if defects are evaluated using AI for these images as they are, probability of errors in defect detection is high. As a pretreatment for detecting anomalies in defects using the AI, we focused on the nondestructive inspection using MO imaging and performed an unprecedented image filter processing. By automatically evaluation the MO images using AI thereafter, the accuracy of defection identification was improved. In this paper, we report on the characteristics of the automatic evaluation with the AI of the MO images obtained from several types of MO elements with varying properties.

II. NON-DESTRUCTIVE INSPECTION USING A MAGNETO-OPTICAL IMAGING SENSOR

A. Characteristics of the magneto-optical imaging sensor

The MO effect is a phenomenon where the polarization plane of light traveling in a magnetic material that is magnetized rotates. For this phenomenon, the relationship between magnitude of magnetization and rotation angle of the polarization plane is shown in (1).

$$\theta_F = F \times (M / M_S) \times L \quad (1)$$

where θ_F is rotation angle of the polarization plane, M_S is saturation magnetization of the MO element, M is the magnitude of magnetization parallel to the traveling direction of light, and L is the distance that light penetrates in the magnetic material (film-thickness of the element). F is called a Faraday rotation coefficient, which is a value specific to the material.

From Equation (1), it can be seen that the larger the magnetization value is, the large the rotation angle of the polarization plane becomes. In other words, the larger a magnetic field applied from the outside becomes, the greater the influence of the MO effect becomes. When a defect exists on the surface of a test subject, the magnetic field leaks in the vicinity of the defect when the object is excited. In the MO imaging, the MO element is used as a magnetic field sensor to sense the magnetic field leaking from the defect. Regarding the material for the MO element, a thin film of magnetic garnet [14]-[15], which is a ferromagnetic material, is generally used. In this study, we used bismuth-substituted yttrium iron garnet (Bi:YIG).

The rotation angle of the polarization plane cannot be seen directly. However, by arranging two polarizers in a crossed Nicols configuration in a way that they sandwich the MO element, the rotation angle can be converted to light intensity. In other words, the rotation angle can be seen as the brightness of the image. The relationship between the rotation angle of the polarization plane and the light intensity (I) is shown in (2).

$$I = I_{in} \times R \times \sin^2\theta_F \quad (2)$$

where I_{in} is the intensity of incident light, R is the reflectance of the MO element, and θ_F is the rotation angle of the polarization plane.

The rotation angle of the polarization plane differs between places where the magnetic field leaks and places where it does not. Thus, by generating an image as the difference in brightness (contrast) via the MO effect, the MO imaging can be used for the nondestructive inspection. The spatial resolution of the MO imaging depends on the size of the magnetic domain of the MO element used as the sensor. Because the magnetic domain can be miniaturized up to the order of nanometers, it has a feature that high spatial resolution, in the order of micrometers, can be obtained by capturing images with a microscope. This is fast and easy because it tests an electromagnetic phenomenon two-dimensionally using light and, and is therefore a useful method for the deep learning with the image processing.

In this study, we prepared the following three types of MO elements with differing characteristics for the automatic evaluation using the AI.

1) Multilayer film‐high spatial resolution type
2) Single-layer film‐ low-remanence type
3) Single-layer film‐ high-remanence type

The high spatial resolution MO element is a multilayer film that uses a magnetophotonic crystal (MPC) [16]-[21]. MPC has a multilayered film structure wherein parts of the periodic structure of a photonic crystal are replaced with the magnetic film layers. It is an artificial magnetic lattice that combines the magnetic film layers and dielectric thin film layers in a cycle approximate to the wavelength of light. Even if the magnetic layer is a thin film, a large MO effect is exhibited. Therefore, obtaining a MO image with high spatial resolution is possible. Two types of transparent thin layer films with different refractive indexes are used for the dielectric multilayer film. In this study, we used SiO_2 as the low-refractive material, and Ta_2O_5 as the high-refractive material.

A high-frequency ion beam sputtering method was used to make the Bi:YIG magnetic film layer. A sintered body of a material into which a large amount of Bi was substituted, i.e., $Bi_{1.5}Dy_{1.0}Y_{1.0}Fe_{3.8}Al_{1.2}O_X$, (4-inch in diameter, 5 mm in thickness) was used for a target. We used a 1-inch substituted gadolinium/gadolinium/gallium substrate. Argon was used as a sputtering gas; oxygen was introduced into the chamber (oxygen blow). After the film was formed, a rapid heating and quenching crystallization thermal treatment was conducted at 700 deg.C for 15 minutes under atmospheric pressure using a tubular electric furnace. The result of composition analysis using an energy dispersive X-ray analyzer showed that the chemical composition after the thermal treatment was $Bi_{1.36}Dy_{1.07}Y_{0.57}Fe_{3.7}Al_{1.3}O_{12}$. Meanwhile, the dielectric multilayer film was prepared under the same conditions as for Bi:YIG using a high-frequency ion beam sputtering method.

A low-remanence MO element is a single-layer thin film, in which the magnetic layer has a uniaxial anisotropy in the direction parallel to the plane. The MO imaging detects the magnetic field leaked from the defect in the vertical direction; therefore, the remanent magnetization in the vertical direction of this MO element is small, thereby capturing the MO image with less noise.

On the other hand, a high-remanence MO element is a single-layer film, in which the magnetic layer has the uniaxial anisotropy in the direction perpendicular to the plane. The MO element is highly sensitive to a stray field leaking vertically from the defect and is greatly affected by a noise from a remanent magnetization. For both single-layer films, we used the MO elements prepared by metal-organic decomposition [22]-[24] purchased from "Off-Diagonal" Co., Ltd..

B. **Magneto-optical imaging method**

For the MO imaging using the high spatial resolution type MO element, the MO images were taken using a polarization spectroscopic microscope to make the best use of its resolution. Fig. 1 shows a schematic diagram of the MO imaging optical system.

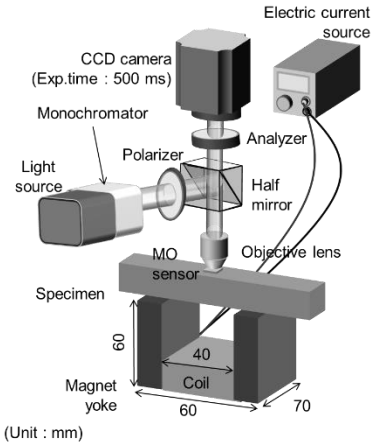

Fig. 1 Schematic diagram of the MO imaging optical system Ⅰ. (For capturing the high spatial resolution element)

The MO element was arranged on the surface of the subject as a sensor for the leaking magnetic field. We used a white xenon lamp as the light source and set the wavelength at 532 nm with a spectroscope. This was the resonance wavelength of MPC, at which high sensitivity can be achieved.

The light that was converted to linearly polarized light through the polarizer was reflected by a half mirror and irradiated toward the MO sensor installed on the surface of the object. The light reflected from the MO sensor was converted to light intensity when it passed through the analyzer arranged in crossed Nicols configuration. Finally, a charge-coupled device image sensor captured the MO image. The magnification of the objective lens we used was 4.

Meanwhile, we used a direct current coil to excite the object and controlled the intensity of the excitation with the current. The number of turns of the coil was 351, and it was set so that the magnetic field of 100 Oe could be obtained with the current of 1 A.

For the MO imaging using the low-remanence and the high-remanence MO elements, we used a smartphone for convenience. Fig. 2 shows the schematic diagram of the optical system. We used a white LED panel as the

light source, and the light that were converted to linearly polarized light through the polarizer.

The light applied to the object was reflected by the MO element and passed through the analyzer. When the light passed through the analyzer, the rotation angle of its polarization plane was converted to the light intensity. Finally, the MO image was captured with the complementary metal oxide semiconductor image sensor installed in the smartphone.

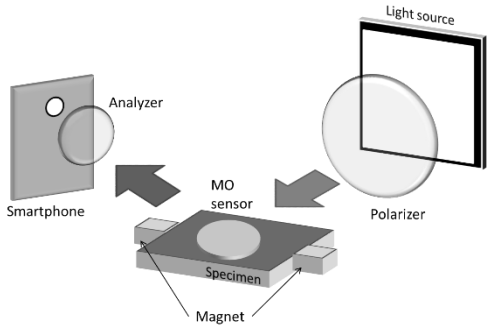

Fig. 2 Schematic diagram of the MO imaging optical system II. (In the case of the low-remanence and the high-remanence elements)

A neodymium magnet was used to excite the test subject, and the intensity of excitation was controlled with the number of magnets. Fig. 3 shows the results of the MO imaging taken with the low-remanence MO element using the optimal system shown in Fig. 2. The schematic diagram of the surface of a SS400 steel sheet we used as the test subject is shown in Fig. 3 (a). The test subject was square-shaped with the size of 10 mm × 10 mm. A slit with 0.5 mm width was made in the center as the defect. Six 0.42 T neodymium magnets were installed as shown in Fig. 3 (a) to excite the test subject. The obtained MO image is shown in Fig. 3 (b). A bright-dark contrast can be observed at the location of the slit on the surface of the MO element, indicating that the defect was visualized.

III. EVALUATION OF DEFECT IN MAGNETOOPTICAL IMAGES USING A DEEP MODEL

We used a variational autoencoder (VAE) [25] as the algorithm of a deep generative model for image processing. Fig. 4 shows the VAE's learning of the MO images and detection of anomalies. Defection-free MO images were learned as the training data to obtain a deep generative model. The MO images with defects were used as the test data next. When MO images with defects that have never been learned is input, only the defective part becomes inconsistent. Then, the difference can be extracted. A heat map is created based on the coordinates obtained.

III. Implementation of the deep generative model

A detection method for anomaly with the deep generative model was applied to the MO image. The learning model was constructed by using TensorFlow at

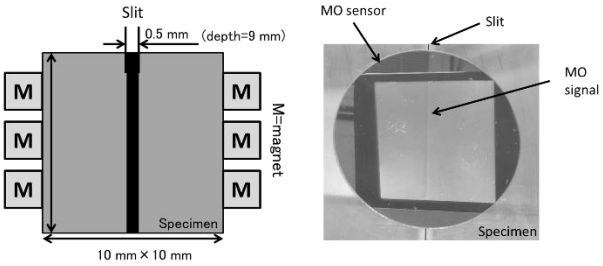

(a) Appearance of the test subject (b) MO image

Fig. 3 MO images taken using the optical system in Fig. 2

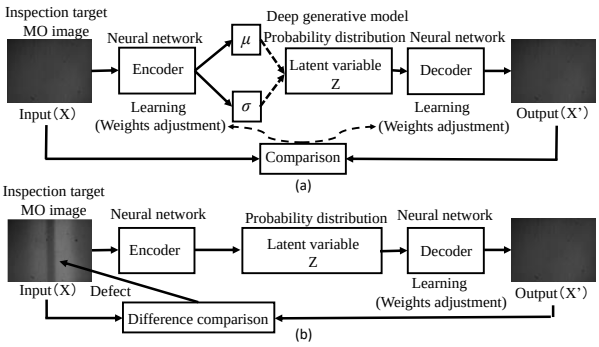

Fig. 4 Learning with the variational autoencoder and detection of anomaly in MO image

the backend of Keras–a deep learning library of Python. The actual test piece was used as the original data set, and both defective and non-defective MO images were used.

IV. Acquiring the MO image for defects evaluation

For "scratch"–a defection detection item, the slit defect with the width of 0.15 mm and the depth of 6 mm. The test subject was a SS400 steel plate. Fig. 5 (a) shows an optical image of the surface captured directly by a smartphone camera. The line visible in the center is the slit defect. Lines were drawn on the left and the right of the slit as noises. Since information other than the scratch

such as dirt is also visualized in the optical image, that causes the noise, making automatic judgment by the AI difficult. The MO image taken using the high-remanence MO element is shown in Fig. 5 (b). Since the magnetic field leaked from the defect is visualized in the MO image, information such as dirt is filtered. This makes it possible to visualize the defect signal only; this is advantageous for the automatic evaluation with the AI.

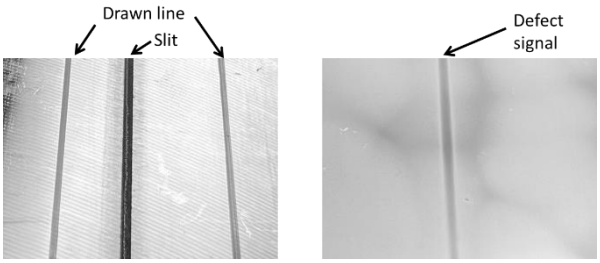

(a) Optical image (b) MO image

Fig.5 Comparison of the optical image and the MO image

Fig. 6 shows the MO images captured with the high spatial resolution MO element. For this experiment, the width and depth of the slit were set to 0.15 mm and 1 mm, respectively, to demonstrate that the high spatial resolution element can detect minute defects. Fig. 6 (a) shows the MO image of the surface of SS400 steel without the defect, and Fig. 6 (b) shows the MO image with the slit defect. It can be observed that it was able to detect the defect based on the white bright spots at both the ends of the slit.

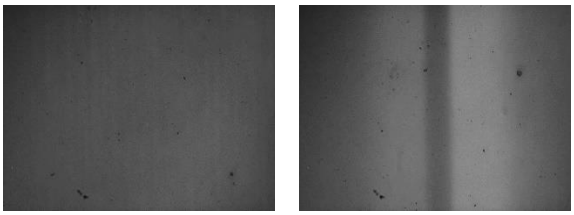

(a) No defect (b) Slit defect

Fig.6 MO images for no defect and slit defect with high spatial resolution MO element

Fig. 7 shows the MO images captured with the low-remanence MO element. Fig. 7 (a) shows the MO image of the surface of SS400 steel without the defect, and Fig. 7 (b) shows the MO image with the slit defect. There was a bright/dark contrast at the location of the slit.

Fig. 8 shows the MO images captured with the high-remanence MO element. Fig. 8 (a) shows the MO image of the surface of SS400 steel without the defect, and Fig. 8 (b) shows the MO image with the slit defect. Similar to the previous results, there was a bright/dark contrast at the location of the slit, indicating that defects can be visualized with MO imaging for all three types of MO elements tested.

V. Defects evaluation using a deep generative model

Defects evaluation with deep generative model was performed using the MO images with the high spatial resolution, the low remanence, and the high-remanence MO elements obtained in the previous section as the input images. For the training data, 100,000 images were prepared by cutting out 8 × 8 images from 28 × 28 MO images without defects.

For the test data, we used a 28 × 28 MO image with a 0.15 mm wide slit defect taken using the high spatial resolution MO element. Regarding the heat map for visualizing the anomalous section, an 8 × 8 small window was scanned vertically and horizontally with 2-pixel increments on the original 28 × 28 image and accumulated. The input MO image was 8-bit grayscale image.

Fig. 9 shows the heat map of the degree of anomaly for the MO image taken using the high spatial resolution MO element. The degree of anomaly was high at the location of the slit.

Fig. 10 shows the heat map of the degree of anomaly for the MO image taken using the low-remanence MO element. The degree of anomaly was higher when the defect was present; however, it was high overall.

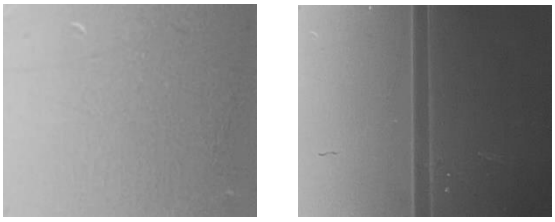

(a) No defect (b) Slit defect

Fig.7 MO images for no defect and slit defect with high spatial resolution MO element

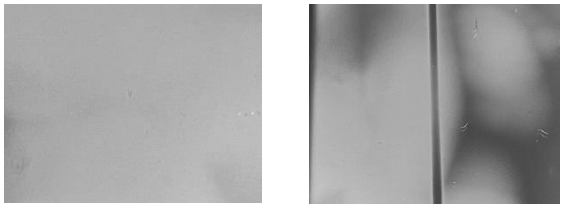

(a) No defect (b) Slit defect

Fig.8 MO images for no defect and slit defect with high spatial resolution MO element

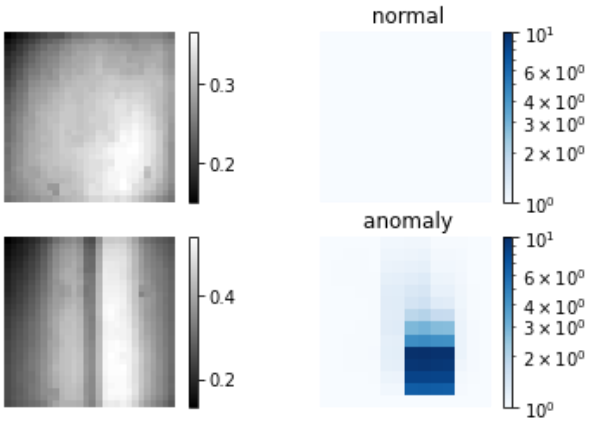

Fig.9 Anomaly heat map for high spatial resolution MO imaging

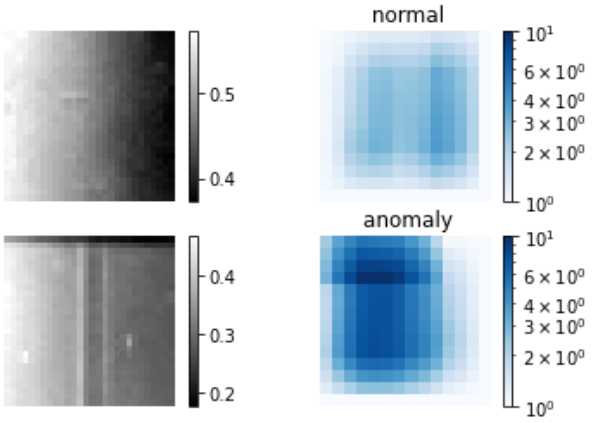

Fig.10 Anomaly heat map for low-remanence MO image

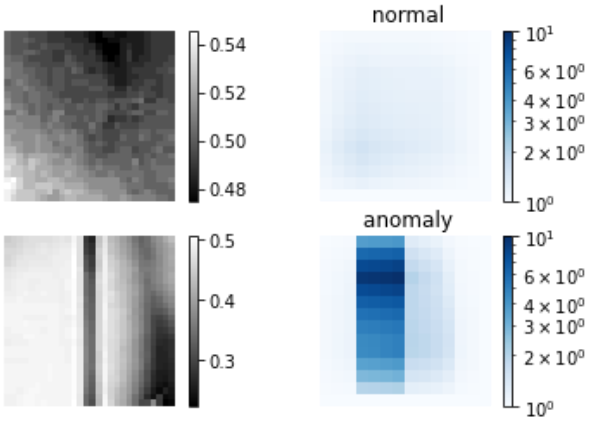

Fig.11 Anomaly heat map for high-remanence MO image

VI. DISCUSSION

Using the MO images with high spatial resolution, the low remanence, and the high-remanence MO elements as the input images, defects evaluation was performed using the deep generative model. For the high spatial resolution MO element and the high-remanence MO element, the degree of anomaly was remarkably high in the slit defect section. However, for the low-remanence MO element, the degree of anomaly was generally high, even in areas outside of the slit defect section. There was owing to a glare of reflected light on the learning data of the MO image without the defect, which affected the creation of the training data.

V. CONCLUSION

The purpose of this study was to develop a technology that automatically detect defects in a plant steel structure by visualizing a “crack” and other defects in the plant steel structure using a MO element as a sensor and subsequently deep-learning the MO image obtained. Using a deep generative model, we succeeded in defects evaluation in the MO images that had slit defects with the width of 0.15 mm and the depth of 6 mm.

In future, considering the definition of the degree of anomaly and setting for threshold values for each defection item, such as corrosion and scratches, is necessary. In addition, it is necessary to further study the size of the MO images and computer processing time toward developing a non-destructive inspection robot that would replace manual inspections..

ACKNOWLEDGMENT

This work was supported by JSPS KAKENHI Grant Number JP19K14851.

REFERENCES

[1] R. Hashimoto, H. Takagi, T. Yonezawa, K. Sakaguchi and M. Inoue, Magneto-optical imaging using magneto photonic crystals, Journal of Applied Physics, 115(17), 17A931, 2014.

[2] R. Hashimoto, T. Yonezawa, H. Takagi, T. Goto, H. Endo, A. Nishimizu and M. Inoue, Defect depth estimation using magneto optical imaging with magnetophotonic crystal, Journal of the Magnetics Society of Japan, 39(5), 213-215. 2015.

[3] G. L. Fitzpatrick, D. K. Thome, R. L. Skaugset, E. Y. C. Shih, and W. C. L. Shin, Magneto-optic/eddy current imaging of aging aircraft: a new NDI technique, Materials Evaluation, 51(12), 1402-1407. 1993.

[4] D. C. van der Laan, H. J. N. van Eck, M. W. Davidson, B. ten Haken. H. H. J. ten Kate and J. Schwartz, Magneto-optical im-aging study of the crack formation in superconducting tapes caused by applied strain, Physica C, 372-376, 1020-1023. 2002.

[5] P. Novotny, P. Sajdl and P.Machac, A magneto optic imager for NDT applications, NDT & E International, 37(8), 645-649. 2004.

[6] P. Y. Joubert and J. Pinassaud, Linear magneto-optic imager for non-destructive evaluation, Sensors and Actuators A, 129(1-2), 126-130. 2006.

[7] H. Murakami and M. Tonouchi, High-sensitive scanning laser magneto-optical imaging system, Review of Scientific Instruments, 81(1), 013701-1-013701-7. 2010.

[8] H. Lee, T. Kim, S. Kim, Y. Yoon, S. Kim, A. Babajanyan, T. Ishibashi, B. Friedman and K. Lee, Magneto-optical imaging using a garnet indicator film prepared on glass substrates, Journal of Magnetism and Magnetic Materials, 322(18), 2722-2727. 2010.

[9] M. Bazijievich, D. Barness, M. Sinvani, E. Perel, A. Shaulov and Y. Yeshurun, Magneto-optical system for high speed real time imaging, Review of Scientific Instruments, 83(8), 083707-1-083707-8. 2012.

[10] X. Gao, Y. Liu and D. You, Detection of micro-weld joint by magneto-optical imaging, Optics & Technology, 62, 141-151. 2014.

[11] X. Gao, Y. Chen, D. You, Z. Xiao and X. Chen, Detection of micro gap weld joint by using magneto-optical imaging and Kalman filtering compensated with RBF neural network, Mechanical System and Signal Processing, 84(A), 570-583. 2017.

[12] X. Gao, N. Ma and L. Du, Magneto-optical imaging characteristics of weld defects under alternating magnetic field excitation, Optical Express, 26(8), 9972-9983. 2018.

[13] P. S. Pershan, Magneto-optical effects, Journal of Applied Physics, 38, 1482-1490. 1967.

[14] T. Suzuki, G. Zaharchuk, G. Gorman, F. Sequeda and P. Labun, Magnetic and magneto-optical properties and crystallization kinetics of rapid-thermally crystallized Bi-substituted garnet films, IEEE Transactions on Magnetics, 26(5), 1927-1929. 1990.

[15] K. Matsumoto, S. Sasaki, Y. Asahara, K. Yamaguchi and T. Fujii, Highly bismuth substituted yttrium iron garnet single crystal films prepared by sol-gel method, Journal of Magnetism and Magnetic Materials, 104-107, 451-452. 1992.

[16] M. Inoue, K. Arai, T. Fuji and M. Abe, Magneto-optical properties of one-dimensional photonic crystals composed of magnetic and dielectric layers, Journal of Applied Physics, 83(11), 6768-6770. 1998.

[17] M. Inoue, T. Fujii, Huge enhancement of the magneto-optical faraday effect of films with disordered multilayer structures supporting the localization of light, Journal of the Magnetics Society of Japan, 21(4-1), 187-192. 1998.

[18] H. Kato, T. Matsushita, A. Takayama and M. Egawa, Theoretical analysis of optical and magneto-optical properties of one-dimensional magnetophotonic crystals, Journal of Applied Physics, 93(7), 3906-3911, 2003.

[19] M. Inoue, R. Fujikawa, A. Baryshev, A. Khanikaev, P. B. Lim, H. Uchida, O. Aktsipetrov, A. Fedyanin, T. Murzina and A. Granovsky, Magnetophotonic crystals, Journal of Physics D: Applied Physics, 39, R151–R161. 2006.

[20] K. Takahashi, F. Kawanishi, S. Mito, H. Takagi, K. H. Shin, J. Kim, P. B. Lim, H. Uchida and M. Inoue, Study on magnetophotonic crystals for use in reflection-type magneto-optical spatial light modulators, Journal of Applied Physics 103(7), 07B331-1-07B331-3. 2008.

[21] K. H. Chung, T. Kato, S. Mito, H. Takagi and M. Inoue, Fabrication and characteristics of one-dimensional magnetophotonic crystals for magneto-optic spatial light phase modulators, Journal of Applied Physics 107(9), 09A930-1-09A930-2. 2010.

[22] T. Ishibashi, A. Mizusawa, M. Nagai, S. Shimizu, and K. Sato, Characterization of epitaxial (Y,Bi)3(Fe,Ga)5O12 thin films grown by metal-organic decomposition method, Journal of Applied Physics, 97(1), 013516-1-013516-4. 2005.

[23] T. Ishibashi, T. Yoshida, T. Kobayashi, S. Ikehara and T. Nishi, Preparation of Y0.5Bi2.5Fe5O12 films on glass substrates using magnetic iron garnet buffer layers by metal-organic decomposition method, Journal of Applied Physics 113(17), 17A926-1-17A926-3. 2013.

[24] T. Ishibashi, Magneto-optical imaging using bismuth-substituted iron garnet films prepared by metal-organic decomposition, Journal of the Magnetics Society of Japan, 44(5), 108-116. 2020.

[25] D. P. Kingma, M. Welling, Auto-Encoding Variational Bayes, ICLR, 2014.